10.1109/ULTSYM.2015.0296

The Contribution of Shear Wave Absorption to Ultrasound Heating in Bones: Coupled Elastic and Thermal Modeling

Bradley E. Treeby*, Teedah Saratoon
Department of Medical Physics and Biomedical Engineering, University College London, London, UK
*Email: b.treeby@ucl.ac.uk

***Abstract*—Precisely quantifying the heating of bone is important in many diagnostic and therapeutic applications of ultrasound. Here, the heating of bone by ultrasound is investigated using an elastic wave model coupled with the bioheat transfer equation. The volume rate of heat deposition is calculated separately for the compressional and shear waves by splitting the acoustic particle velocity during the simulation using a k-space dyadic. Four bone geometries of increasing complexity are studied for both plane piston and focused bowl transducers. Close to normal incidence, the heating is dominated by the absorption of compressional waves. Under these conditions, both fluid and elastic models give similar predicted temperature rises. As the angle of incidence is increased beyond 10 degrees, the contribution from shear wave absorption becomes significant. For the plane piston transducer, there is a sharp drop in compressional wave heating around the critical angle. In contrast, using a focused transducer, the reduction in compressional wave heating with angle is much smoother, extending well beyond the critical angle.**

I. Introduction

There are many applications of therapeutic ultrasound in which ultrasound waves interact with bone. These include high-intensity focused ultrasound (HIFU) therapies delivered through the ribs or skull, HIFU treatments targeted at bone metastasis for pain relief, and low-intensity ultrasound used in physiotherapy. In these applications, the heating of bone and surrounding tissue needs to be controlled; either to avoid thermal damage, or to ensure adequate treatment delivery. Compared to soft tissue, the heating of bone is complicated by the presence of a fluid–solid interface. In this case, the generation, propagation, and absorption of shear waves within the bone must also be considered [1]. The absorption in bone is considerably higher than in the surrounding soft tissue, and the shear absorption coefficient is approximately twice that of the compressional wave [2]. Previous studies have shown that at moderate angles of incidence, heating in bone is dominated by shear wave absorption [1, 3]. The specific absorption rate is highest at the bone interface, with the peak temperature located within the bone close to the interface [4, 5].

Studies into bone heating typically combine a model of ultrasound propagation with the bioheat transfer equation to calculate heat diffusion. The ultrasound model is either treated analytically assuming plane wave incidence and an idealized bone surface such as a half-space or layered medium, e.g., [1, 3–5], or numerically using a model of ultrasound propagation with the bone geometry derived from patient data, e.g., [6, 7]. In the latter case, the contribution of shear waves is often neglected due to computational constraints. The current work is a preliminary investigation bridging these two approaches to establish to what extent the effects observed in an idealized situation also apply to realistic bone geometries and source conditions.

This work was supported in part by the European Metrology Research Programme (EMRP), and the EPSRC, UK. The EMRP is jointly funded by the EMRP participating countries within EURAMET and the European Union.

II. Coupled Elastic Thermal Modeling

A. Numerical Model

The elastic wave simulations were performed in 2D using the Kelvin-Voigt elastic wave model (`pstdElastic2D`) in the open-source k-Wave MATLAB Toolbox [8]. Four geometries of increasing complexity representative of the shaft (diaphysis) of a long bone were considered as shown in Fig. 1. The first was a fluid-elastic half-space in which the lower half-space was assigned the properties of bone. The second was a solid bone layer with a thickness of 26 mm. These geometries are often used in analytical investigations. The third was a hollow bone layer of the same outer diameter, with a compact bone thickness of 6 mm, and a marrow cavity thickness of 14 mm. The fourth was segmented from a CT scan of the femur using the freely available KESKONRIX dataset (http://www.osirix-viewer.com/datasets). The elastic and thermal properties used in the simulations were derived from [2] and are given in Table I. Each simulation was also repeated with the shear properties set to zero to investigate when using a fluid model is sufficient to model heating in bones.

For each bone geometry, two different source configurations were investigated. The first was an unfocused plane piston transducer with a diameter of 50 mm. The second was a focused bowl transducer with a diameter of 64 mm and a radius of curvature of 94 mm (matching the Sonic Concepts H-151 transducer). Both were driven with a continuous wave sinusoid at 1.1 MHz with a surface intensity of 4 $\mathrm{W\,cm^{-2}}$, giving a focal intensity of 37 $\mathrm{W\,cm^{-2}}$ for the focused transducer. The angle of incidence to the bone was varied from 0° (normal incidence) to 60° as shown in Fig. 1. The transducers were positioned such that the geometric focus of the bowl transducer was in the center of the bone layer (shown with a black dot in Fig. 1).

The simulations were performed on a 2D Cartesian grid with a grid size of 1024 × 1536 and a grid spacing of 125 μm. This corresponds to 10.4 grid points per wavelength at the slowest wave speed. The simulations were run for 140 μs (which allowed the simulations to reach an approximately steady state) with a time step of 9.1 ns, giving 100 points per period at the driving frequency and 15,401 total time steps. A

978-1-4799-8182-3/15/$31.00

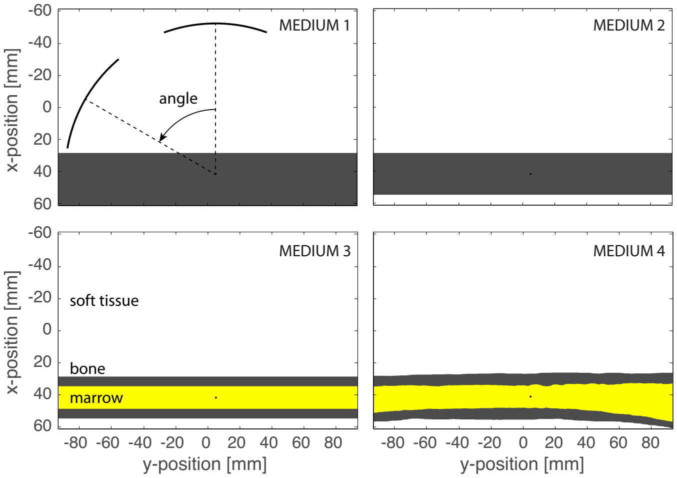

Fig. 1. Four long-bone geometries used in numerical experiments: (1) half space, (2) solid bone layer, (3) hollow bone layer, and (4) anthropometric bone layer derived from a segmented CT scan. For each geometry, simulations were performed using focused bowl and plane piston transducers at angles of incidence from 0° (normal incidence) to 60°.

TABLE I. MATERIAL PROPERTIES USED IN THE SIMULATIONS.

	Soft Tissue	Bone	Marrow	
density	1090	1900	928	kg/m^3
sound speed compression	1580	2820	1430	m/s
sound speed shear	-	1500	-	m/s
absorption compression	0.57	9	0.6	$dB/(MHz^2 cm)$
absorption shear	-	20	-	$dB/(MHz^2 cm)$
specific heat	3400	1300	2740	J/(kg.K)
thermal conductivity	0.5	0.3	0.22	W/(m.K)

perfectly matched layer with a thickness of 20 grid points was used to simulate free-field conditions. The simulations were run using a GeForce GTX Titan X graphics processing unit (GPU) with 3072 CUDA cores and 12 GB of GDDR5 memory (NVIDIA Corporation, CA, USA). Each elastic simulation took 9 minutes to run and used 11.45 GB of memory.

For each simulation, the volume rate of heat deposition Q was calculated from the steady state particle velocity amplitude $\mathbf{u}$ according to the plane wave relationship $Q = \alpha I_{\text{av}} = \alpha \rho_0 c_0 u^2$, where $u^2 = \mathbf{u} \cdot \mathbf{u}$, α is the absorption coefficient in Np/m, ρ_0 is the mass density, and c_0 is the sound speed. Due to the different material parameters for compressional and shear waves, the individual contributions to the heating term were computed by splitting the particle velocity into compressional (P) and shear (S) components during the simulation using a k-space dyadic [9], and storing these separately. The volume rate of heat deposition in W/m^3 at each grid point was then calculated using $Q_{\text{P}} = \alpha_{\text{P}} \rho_0 c_{\text{P}} u_{\text{P}}^2$ and $Q_{\text{S}} = \alpha_{\text{S}} \rho_0 c_{\text{S}} u_{\text{S}}^2$, with the total heat deposition given by $Q_{\text{total}} = Q_{\text{P}} + Q_{\text{S}}$.

The elastic wave simulations were coupled to a thermal simulation using the steady state volume rate of heat deposition. The thermal model was based on a heterogeneous extension to the exact solution of the bio-heat equation given in [10]. The model is analogous to the k-space pseudospectral solution for the wave equation used in the k-Wave toolbox, and allows the diffusion of heat in heterogeneous tissue to be calculated in a computationally efficient manner. The model is exact in the case of homogeneous media, and gives high accuracy for low computational cost in the case of heterogeneous coefficients. The thermal simulations were run on the same spatial grid as the elastic simulations with a time step of 50 ms, a total heating time (sonication length) of 5 s, a background temperature of 37°C, and no perfusion. The simulations were performed using an Intel Xeon E5-2620 hex-core CPU running at 2.4 GHz and each simulation took 20 s to run.

For each bone geometry, source condition, and sonication angle, the peak volume rate of heat deposition within the bone (calculated from the elastic model), and the peak temperature within the bone (calculated from the thermal model) were extracted. The peak values were taken as the average over the highest 64 grid points (corresponding to 1 mm^2), excluding a 1 mm boundary layer from the top surface of the bone.

B. Results

The final temperatures for sonication angles of 0°, 20°, 40°, and 60° are shown in Fig. 2. The top rows in Fig. 2(a) and Fig. 2(b) show the results for the solid bone layer using a fluid model instead of an elastic model (i.e., with the shear properties set to zero). The final temperatures for the half-space are not shown as they were indiscernible from the solid bone. The corresponding compressional and shear wave contributions to the peak volume rate of heat deposition and the peak temperature inside the bone layer as a function of angle are shown in Fig. 3.

Close to normal incidence, there is very little mode conversion from compressional waves in the soft tissue to shear waves inside the bone, and thus the contribution of shear wave absorption to heating is close to zero. Under these conditions, the final temperatures predicted by the fluid and elastic models are very similar. However, as the angle is increased beyond 10°, heating from the generation and absorption of shear waves becomes an important component of the total heat deposition (Fig. 3). Beyond 40°, there is a significant difference in the temperature maps when shear waves are neglected (3°C for the piston transducer, and 10°C for the bowl transducer). In this case, the fluid model incorrectly predicts that a large component of the acoustic energy is reflected from the bone surface, and thus underestimates the acoustic energy absorbed in the bone.

For the material properties used here, the critical angle for the compressional wave assuming plane wave incidence is 34° (shown with a dotted line in Fig. 3). For the plane piston transducer, there is a sharp drop in heating from the absorption of compressional waves around this angle. For the focused transducer, the reduction is much smoother, and as a result, the increase in shear wave heating is also less pronounced. Neither source condition results in a significant drop in total energy transmission at the first critical angle as might be predicted under a plane wave assumption [5].

The high absorption within the bone means the penetration depth of the ultrasound waves is relatively short. Consequently, for the sonication conditions considered, there is not a major difference in the volume rate of heat deposition or peak temperature as the complexity of the bone geometry is increased. However, for the bone geometries including the marrow layer, the temperature increase is almost entirely constrained to the upper layer of compact bone (this is particularly visible for the temperature maps in Fig. 2(b)).

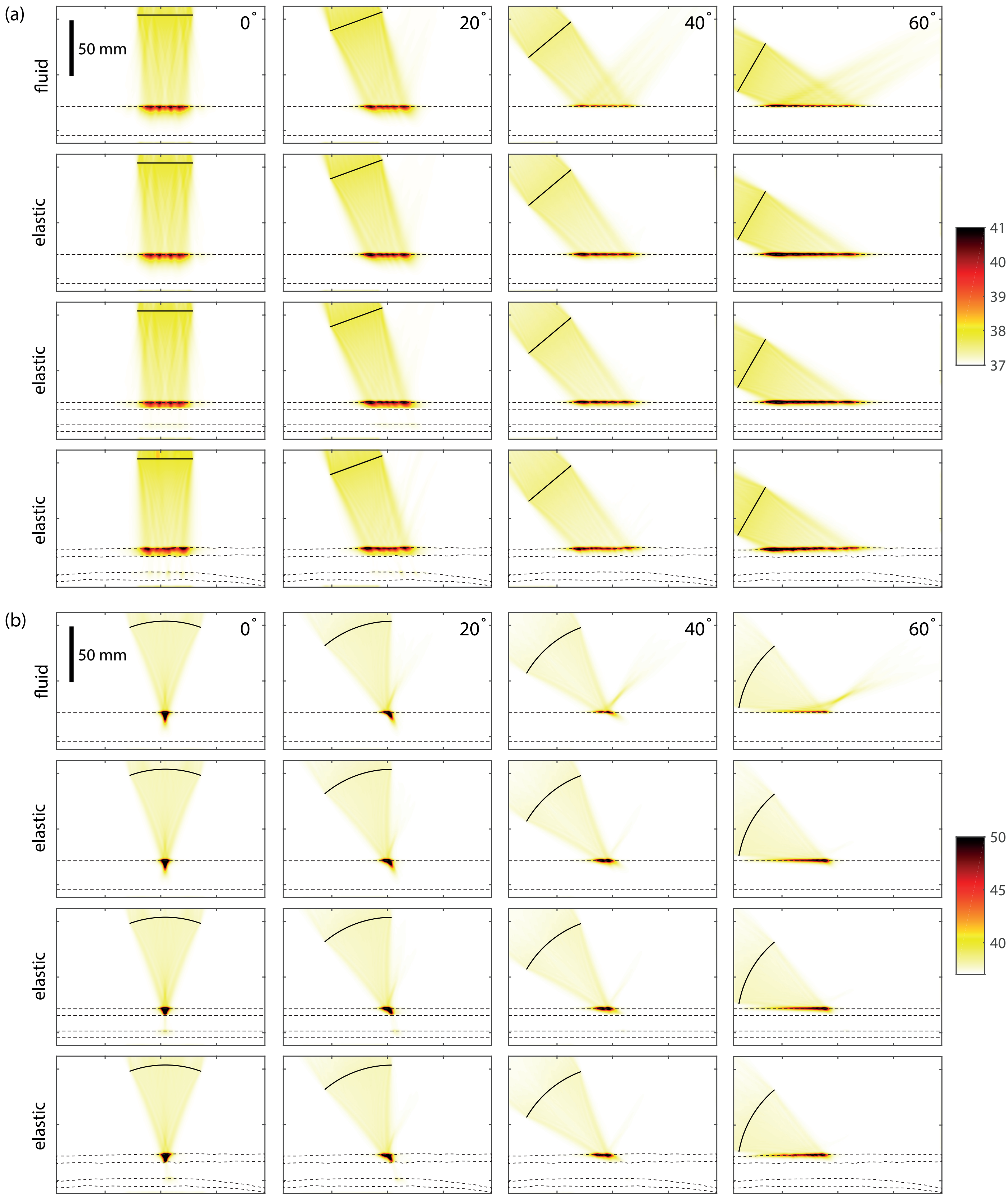

Fig. 2. Final temperature field for (a) plane piston, and (b) focused bowl transducers for four different sonication angles and three different bone geometries of increasing complexity (medium 2, 3, and 4 shown in Fig. 1). The dotted lines show the location of the bone layer. The first row for each transducer are simulations with the shear properties set to zero (equivalent to using a fluid rather than elastic model). The heating is primarily restricted to a thin layer around the bone surface due to the high absorption within the bone. For large angles of incidence, the fluid model incorrectly predicts that a large component of the acoustic energy is reflected from the bone surface.

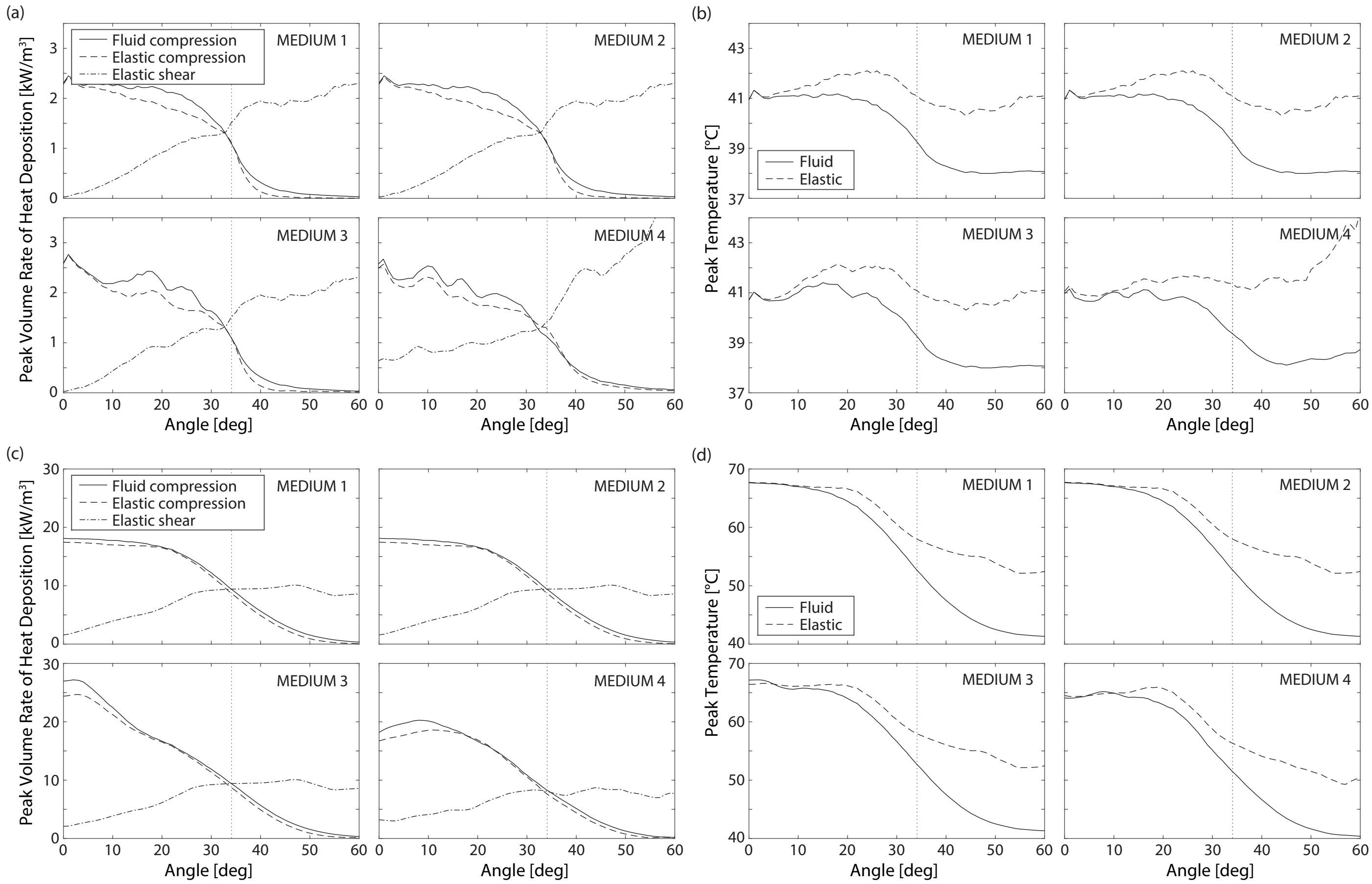

Fig. 3. (a) Peak volume rate of heat deposition within the bone layer for the plane piston transducer as a function of angle for the four medium geometries shown in Fig. 1. The solid line is from the fluid model, and the dashed lines the shear and compressional components from the elastic model. The vertical dotted line is the critical angle for the compressional wave. (b) Peak temperature within the bone layer predicted by the fluid and elastic models. (c)-(d) Equivalent results for the focused bowl transducer.

III. Conclusion

The developed modeling tools make it easy and computationally efficient to study the heating of bones for different sonication conditions and bone geometries. In particular, the models allow the contribution from compressional and shear wave heating to be assessed independently. Close to normal incidence, both fluid and elastic models give similar predicted temperature rises. However, as the angle of incidence is increased, the contribution from shear wave absorption becomes significant. Using a plane piston transducer, there is a noticeable reduction in heating from compressional waves when the angle of incidence is increased beyond the critical angle. In contrast, using a focused transducer, the reduction in heating from compressional waves with angle is much smoother, extending well beyond the critical angle. In future, this work will be extended to examine realistic bone geometries in 3D.

References

[1] B. A. Haken, L. A. Frizzell, and E. L. Carstensen. Effect of mode conversion on ultrasonic heating at tissue interfaces. *J. Ultrasound Med.*, 11(8):393–405, 1992.

[2] F. A. Duck. *Physical Properties of Tissue: A Comprehensive Reference*. Academic Press, New York, 1990.

[3] A. K. Chan, R. Sigelmann, and A. W. Guy. Calculations Of therapeutic heat generated by ultrasound in fat-muscle-bone layers. *IEEE Trans. Biomed. Eng.*, 21(4):280–284, 1974.

[4] M. Fujii, K. Sakamoto, Y. Toda, A. Negishi, and H. Kanal. Study of the cause of the temperature rise at the muscle-bone interface during ultrasound hyperthermia. *IEEE Trans. Biomed. Eng.*, 46(5):494–504, 1999.

[5] W. L. Lin, C. T. Liauh, Y. Y. Chen, H. C. Liu, and M. J. Shieh. Theoretical study of temperature elevation at muscle/bone interface during ultrasound hyperthermia. *Med. Phys.*, 27(5):1131–1140, 2000.

[6] C. W. Connor and K. Hynynen. Patterns of thermal deposition in the skull during transcranial focused ultrasound surgery. *IEEE Trans. Biomed. Eng.*, 51(10):1693–706, 2004.

[7] A. Pulkkinen, Y. Huang, J. Song, and K. Hynynen. Simulations and measurements of transcranial low-frequency ultrasound therapy: skull-base heating and effective area of treatment. *Phys. Med. Biol.*, 56(15):4661–4683, 2011.

[8] B. E. Treeby, J. Jaros, D. Rohrbach, and B. T. Cox. Modelling Elastic Wave Propagation Using the k-Wave MATLAB Toolbox. In *IEEE International Ultrasonics Symposium*, 146–149, 2014.

[9] B. E. Treeby and B. T. Cox. Modeling power law absorption and dispersion in viscoelastic solids using a split-field and the fractional Laplacian. *J. Acoust. Soc. Am.*, 136(4):1499, 2014.

[10] B. Gao, S. Langer, and P. M. Corry. Application of the time-dependent Green's function and Fourier transforms to the solution of the bioheat equation. *Int. J. Hyperthermia*, 11(2): 267–285, 1995.